Inorganic Chemistry

pubs.acs.org/IC Article

Unraveling the Effects of Cobalt on Crystal Growth and Solution Behavior of $Nb_6P_2W_{12}$-based Dimeric Clusters

Dongdi Zhang, Jiancheng Luo, Yachun Ma, Tong Zhang, Nan Li, Chen Li, Pengtao Ma, Tao Li, Guan Wang, Tianbo Liu,* Jingping Wang, and Jingyang Niu*

Cite This: *Inorg. Chem.* 2020, 59, 6747−6754 Read Online

ACCESS | Metrics & More | Article Recommendations | Supporting Information

ABSTRACT: We report the synthesis, characterization, and solution self-assembly of plenary $Nb_6P_2W_{12}$-based transition-metal substituted polyoxometalate, which is obtained by simply adding transition metals (Co^{2+}) into aqueous solution containing cluster $[(NbO_2)_6P_2W_{12}O_{56}]^{12-}$, which is obtained by an in situ synthetic method. The incorporation of Co^{2+} ions significantly affects the crystal structure, resulting in the formation of a 1D chain-like crystal and the first example of a niobotungstate-based cobalt derivative cluster. The behavior and stability of this cluster in solution are confirmed by time-resolved static light scattering, dynamic light scattering, small-angle X-ray scattering, and electrospray mass spectrometry studies.

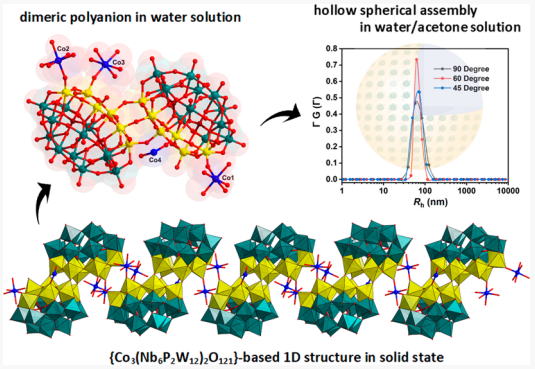

INTRODUCTION

Polyoxometalates (POMs), a large class of anionic metal-oxo clusters,[1,2] have received wide attention owing to their versatile structures and diversity of applications in many areas, including catalysis, magnetism, biomedicine, materials science, and nanotechnology.[3−9] The overall structures of the clusters are based on the edge- and corner-sharing $\{MO_x\}$ polyhedra, where M stands for the group 5 or 6 elements with d^0 electronic configuration (mainly Mo^{VI}, W^{VI}, V^V, Nb^V).[10−17] Mixed-addenda POMs (MAPs) can be formed by the substitution of one or more addendum atoms into metal oxide frameworks due to their similar coordination character. A subset of MAPs is niobotungstate, which was first reported by Dabbabi et al. in 1976.[18] In general, the polyoxoanion can be regarded as a Lewis base and the substitution of W^{VI} by the lower Nb^V results in an increase of electron density and thus the enhanced basicity of the terminal oxygen atoms bonded to niobium,[19−21] which are the potential reactive sites toward electrophilic reagents and can be fused into oligomers by forming Nb−O−Nb linkages. Finke[19] and Hill[22−24] have pioneered the study of Keggin tungstosilicate-based MAPs. Subsequently, Liu reported the preparation of tungstogermanate[25,26] and tungstoarsenate[27] analogues. In recent years, Wang and Zhang presented several Keggin-type tungstosilicate-based transition-metal dimeric[28] and trimeric[29,30] derivatives, respectively. On the other hand, the class of Wells−Dawson-type tungstophosphate-based MAPs was pioneered by Hill,[31] He,[32] and Niu.[33−35] Table S1 lists the previously reported niobotungstate-based cluters formed by Nb−O−Nb linkages. So, it is not surprising that, at least theoretically, the greater the number of Nb atoms in a polytungstate, the higher nucleophilicity can be achieved, and therefore, it is necessary and important to understand the reactions of electrophilic transition-metal ions with Nb/W MAP species, as they bridge the gap between the MAPs and "traditional" transition-metal-substituted POMs (TMSPs).

Among the several Lindqvist, Keggin, and Well−Dawson structure-type Nb/W units we considered, the Wells−Dawson $[(NbO_2)_6P_2W_{12}O_{56}]^{12-}$ cluster, $\{(NbO_2)_6P_2W_{12}\}$ for short, reported by Hill et al. as early as 1997,[31] appears to be a promising building unit precursor because it possesses the largest niobium-oxo cluster among all the primary Nb/W clusters, providing more active sites to incorporate TM ions.[29,35] Moreover, the novel giant POM assemblies can be expected by using the relatively big $\{(NbO_2)_6P_2W_{12}\}$ cluster as a building block.

Taking advantage of all this previous knowledge as well as our ongoing interest in POM chemistry,[36−38] we are now in the position of using the $\{(NbO_2)_6P_2W_{12}\}$ building unit formed in situ as a platform for designing and synthesizing novel clusters, and a series of $\{(NbO_2)_xNb_{6-x}P_2W_{12}\}$-based derivatives has also been isolated from aqueous solution. We report the discovery of the first examples of Wells−Dawson-

Received: December 20, 2019
Published: April 6, 2020

https://dx.doi.org/10.1021/acs.inorgchem.9b03700
Inorg. Chem. 2020, 59, 6747−6754

type-based dimeric and tetrameric niobotungstate assemblies.[33,34] Similarly, we have recently presented a hexameric manganese cluster, $\{Mn_{15}(Nb_6P_2W_{12})_6\}$, which is the first phosphoniobotungstate-based TMSP with single-molecule magnet behavior and also the largest niobotungstate POM reported to date.[35] It can clearly be expected that much more amazing $\{(NbO_2)_6P_2W_{12}\}$-based TMSP structures should be obtained if we explore the synthetic parameter of 3d or 4f metal ions toward the $\{(NbO_2)_6P_2W_{12}\}$ cluster in a more detailed way.

Recently, there has been intense interest among cobalt-based POM derivatives as materials for magnetism and water oxidation catalysis.[39−42] However, no known Co-based MAP has been reported up to now. Herein, a MAP-based cobalt derivative, $(TMA)_2K_5[H_5(Nb_6P_2W_{12})_2Co_3(H_2O)_{11}O_{121}]\cdot 31H_2O$ (**1**, $(TMA)_2K_5$-**1a**$\cdot 31H_2O$), is first synthesized by utilizing a simple synthetic strategy. The solid-state structure was fully characterized by single-crystal X-ray diffraction analysis (Table S2), as well as by IR, TG, and elemental analyses. Polyanion **1a** is comprised of an infinite zigzag chain formed by unprecedented dimeric 12-niobium-24-tungstate $\{Nb_{12}P_4W_{24}\}$ units, which in turn is coordinated to three cobalt ions and therefore represents the first "Co" derivative of MAP. Solution-state speciation of **1a** was determined by electrospray ionization mass spectrometry (ESI-MS), static light scattering (SLS), dynamic light scattering (DLS), and small-angle X-ray scattering (SAXS).

RESULTS AND DISCUSSION

Synthesis. To date, only several isolated Wells−Dawson tungstophosphate-based MAP monomer,[19,31] dimer,[32−34] or tetramer[33,34] polymers have been documented in the literature, and the high dimensional structure containing a $\{(NbO_2)_6P_2W_{12}\}$ unit has never been reported. We have long been involved in a quest to introduce TM cations into the PONb system; in this study, the first characterized 1D chain MAP cluster based on the $\{(NbO_2)_6P_2W_{12}\}$ building block was prepared by a simple, one-pot procedure involving dropwise addition $CoCl_2$ solution to the "saturated" $\{(NbO_2)_6P_2W_{12}\}$ obtained in the presence of H_2O_2 (Scheme 1). The synthetic conditions of compound **1** were also compared with those of its MAP analogues, which contain a similar $\{(NbO_2)_6P_2W_{12}\}$ building block. As shown in Scheme 1, the remarkable differences are pH, temperature, and heating time instead of the molar ratio of polyanion precursors. First, we investigated the two main synthetic conditions. The reaction between $[Nb_6O_{19}]^{8-}$ (Nb_6O_{19}) and $[H_2P_2W_{12}O_{48}]^{12-}$ (P_2W_{12}) with a molar ratio of 1:1 at pH 2.0 and room temperature gave monomeric complex $\{(NbO_2)_6P_2W_{12}\}$ reported by Hill in 1997,[31] while the same reaction at pH 1.85 and 70 °C for 3 h and pH 2.0 and 70 °C for 6 h gave dimeric complex $\{Nb_6(O_2)_2P_2W_{12}O_{59}\}_2$ and $\{Nb_6(O_2)_4P_2W_{12}O_{57}\}_2$ reported by He and our group in 2014[32] and 2015,[34] respectively. As we previously reported, the color of the starting $Nb_6O_{19}/P_2W_{12}/H_2O_2$ solution is bright-yellow, which will turn to light-yellow and finally colorless upon heating.[34] And, the lower the pH is, the shorter the required heating time is. For example, it takes about 48 (pH 2.4) and 36 (pH 2.0) hours for the same reaction system to turn to colorless; however, it can be completely faded within a shorter time (8−10 h) if the pH value is ca. 1.7. In addition, increasing the temperature to 80 °C for 10 h yields the tetrameric $\{Nb_4O_{10}(Nb_6P_2W_{12}O_{61})_4\}$,[33] suggesting that the higher temperature is in favor of the reduction of peroxo groups through thermal decomposition. Second, the results of this study indicate that the $\{(NbO_2)_6P_2W_{12}\}$ fragment described herein can act as basic unit to coordinate transition-metal ions and thus provide a synthetic route to a new class of MAPs-based of TMSPs. As expected, the reaction of $\{(NbO_2)_6P_2W_{12}\}$ and Mn(II) with the molar ratio of 1:10 at pH 2.4 and 90 °C for 10 h leads to the formation of the hexameric $\{Mn_{15}(Nb_6P_2W_{12})_6\}$ anion.[35] Complex **1** could be synthesized by extending the heating time at 90 °C, slightly lowering the pH to 2.2 and increasing the $Nb_6O_{19}/Co(II)/\{(NbO_2)_6P_2W_{12}\}$ ratio. Third, polyanion **1a** can be perfectly crystallized with the addition of tetramethylammonium (TMA^+) counterions; however, powder crystalline can be obtained with the addition of Cs^+ or K^+, indicating that proper counter-cations are imperative to precipitate pure-phase POMs.[43] Therefore, it again shows that small changes in reaction conditions, such as such as pH, temperature, and the amount of materials and counterions, can yield totally different results. Additionally, compound **1** can be obtained by using copper nitrate or copper chloride, showing that the type of cobalt source has no influence on the composition of the final product. Therefore, we think the $(NbO_2)_6P_2W_{12}/H_2O_2/TM^{n+}$ ternary system described herein seems to be of great potential and may open a synthetic route to related species by replacing the Co for other transition-metal or lanthanide ions.

Scheme 1. Main Synthetic Conditions That Result in the Previously Reported Wells−Dawson-Type $P_2W_{12}Nb_6$-Based Polyanions and Cluster 1a Presented Herein

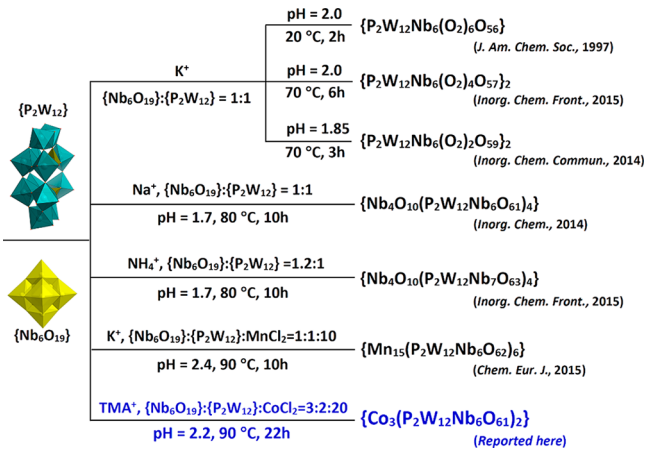

Structural Description. Single-crystal X-ray diffraction analysis reveals that polyanion **1a** is an unprecedented cobalt(II)-containing MAP that crystallizes in a triclinic system (space group $P\bar{1}$). From the viewpoint of structure, the dimeric cluster **1a** is based on a saturated Dawson MAP building units (Figure S1), while the starting material is the lacunary-Dawson species P_2W_{12}, indicating that six Nb(V) ions should be first inserted into the vacant site of each P_2W_{12} before the assembly of cluster **1a**. Compared to the classical Wells−Dawson $[\alpha$-$P_2W_{18}O_{62}]^{6-}$ (P_2W_{18}) fragment, the charge density of $\{(NbO_2)_6P_2W_{12}\}$ unit is unevenly distributed and thus the attached oxo ligands of Nb center have a relatively higher nucleophilicity, which is prone to coordinating with electrophiles (Figure 1).

Details of the structural motif are shown in Figure 2. Polyanion **1a** consists of the $Nb_{12}P_4W_{24}$ hetero-MAP coordinated to four Co^{2+} supporting ions (Figure 2a). The

https://dx.doi.org/10.1021/acs.inorgchem.9b03700
Inorg. Chem. 2020, 59, 6747−6754

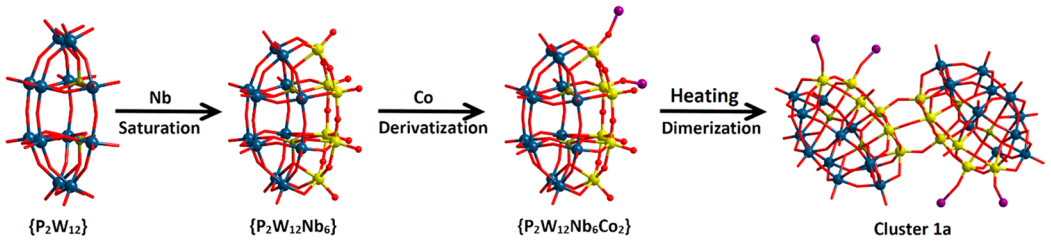

Figure 1. Possible formation process of polyanion **1a** from the viewpoint of structure. All cations and crystal waters are omitted for clarity. Color code: W, teal spheres; Nb, yellow spheres; P, dark-yellow spheres; Co, violet spheres; O, red spheres.

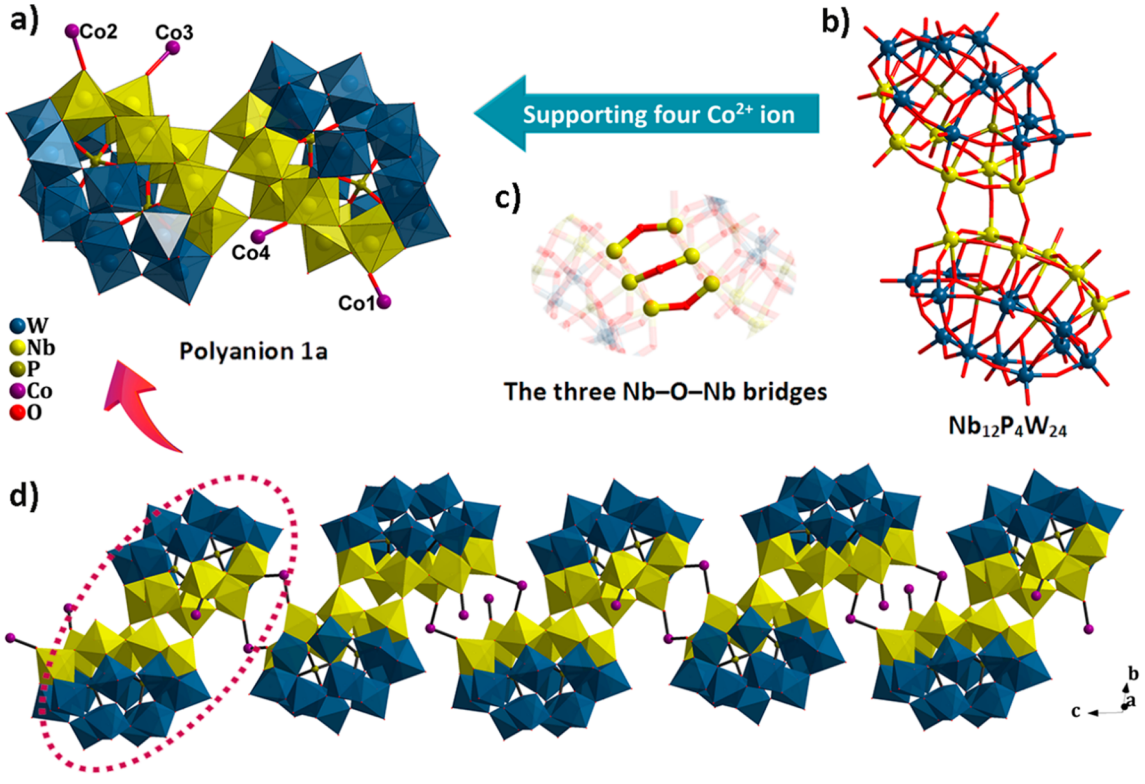

Figure 2. Combined polyhedral/ball-and-stick representation of polyanion **1a** (a), $Nb_{12}P_4W_{24}$ hetero-MAP fragment (b), the three corner-sharing Nb−O−Nb bridges (c), and 1D chain structure in solid state (d). All cations and crystal waters are omitted for clarity. Color code: $\{WO_6\}$, teal octahedra; $\{NbO_6\}$, yellow octahedra; W, teal spheres; Nb, yellow spheres; P, dark-yellow spheres; Co, violet spheres; O, red spheres.

$Nb_{12}P_4W_{24}$ hetero-MAP (Figure 2b) is composed of two identical units $Nb_6P_2W_{12}$ connected by three μ_2-O atoms bonded to niobium centers (two equatorial and one vertical, Figure 2c). Thus, the structure of cluster **1a** can also be simplistically viewed as two reversed $Nb_6P_2W_{12}Co_2$ halves linked together by three Nb−O−Nb linkages (Figure S2). In the cluster, **1a** acts as a ligand for four cobalt centers, which are linked to four terminal oxygen atoms of two belt niobium atoms and two cap ones in $Nb_{12}P_4W_{24}$ hetero-MAP aggregate, respectively. Further, polyanions **1a** are interconneted by Co1 and Co2 centers, forming 1D chain arrangement of the polyanions in solid state (Figure 2d). For the two linker Co ions (Co1 and Co2), the remaining coordination sphere of each cobalt center is completed by four additional water ligands, exhibiting an usual octahedral geometry with coordination number of six. For the two supporting metals, the Co3 ion has five terminal aqua ligands with an distorted octahedral geometry, whereas the Co4 ion only has one terminal aqua ligand, resulting in an unusual two-coordinated Co center (Figure S3). However, the bond lengths of Co−O are within the usual ranges (Table S3).[44] To our knowledge, this is the first example of a niobotungstate cobalt derivative in POM chemistry.

Polyanion **1a** is structurally related to the dimeric $Nb_6P_2W_{12}$-based polyanions, $\{P_2W_{12}Nb_4(NbO_2)_2O_{59}\}_2$ (**2a**)[32] and $\{P_2W_{12}Nb_2(NbO_2)_4O_{57}\}_2$ (**3a**)[34] reported by Yue and Niu et al. in 2014 and 2015, respectively. The structures of **1a**, **2a**, and **3a** are compared to each other from the following three aspects: the dimerization bridges, the reduction of peroxide groups, and the existence of transition metal center or not (Figures 3 and S4). First, the peroxo group in the $\{(NbO_2)_6P_2W_{12}\}$ unit are all reduced to hydroxo groups in **1a**, whereas only four contiguous longitudinal strips of peroxo groups in **2a** and two peroxo groups in the belt sites in **3a** are reduced into hydoxo groups, respectively. Second, the two halves $\{P_2W_{12}Nb_4(NbO_2)_2O_{59}\}$ and $\{P_2W_{12}Nb_2(NbO_2)_4O_{57}\}$ in **2a** and **3a** are both linked together by two μ_2-O atoms bonded to two Nb centers in the same belt position of each halves, but with a *trans*- and *cis*-dimeric configuration, respectively. However, the two TM-coordinated $Nb_6P_2W_{12}Co_2$

https://dx.doi.org/10.1021/acs.inorgchem.9b03700
Inorg. Chem. 2020, 59, 6747−6754

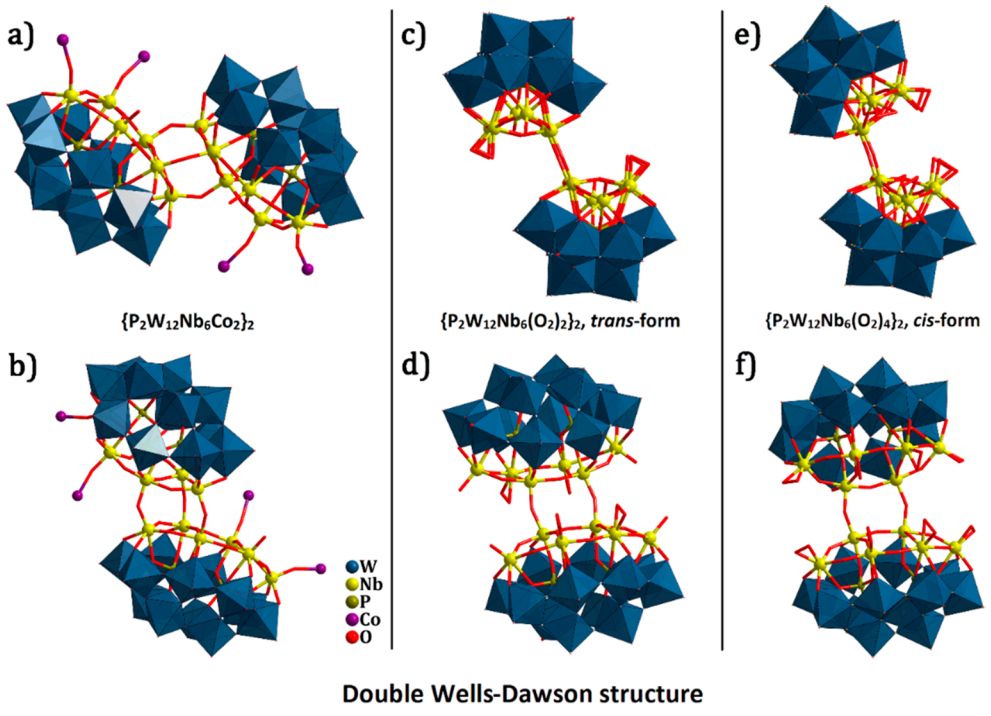

Figure 3. Combined polyhedral/ball-and-stick representation of clusters **1a** (a and b), **2a**[32] (c and d), and **3a**[34](e and f), highlighting the connection mode between the two monomeric building units. All cations and crystal waters are omitted for clarity. Color code: {WO_6}, teal octahedra; {NbO_6}, yellow octahedra; W, teal spheres; Nb, yellow spheres; P, dark-yellow spheres; Co, violet spheres; O, red spheres.

subunits are fused via three Nb−O−Nb bridges in a head−tail staggered way. Interestingly, such dimers share two Co^{2+} linkers with their neighbors, resulting in a 1D chain structure (Figure S5). This is the first observation of MAP-based 1D chain nanocluster constructed from a double-Dawson-type polyoxoanion and cobalt bridges, which may provide an opportunity to further design new structure for the polyanion chemistry of transition metals.

To accurately determine the formula of compound **1**, single-crystal X-ray diffractions, bond valence sum (BVS) calculations (Table S4),[45] and elemental analyses are carried out. Crystallographic refinement indicates that the cobalt occupancy factors in the Co3 and Co4 sites are both 0.5, leading to the formula $[(Nb_6P_2W_{12})_2Co_3(H_2O)_{11}O_{121}]^{12-}$, whereas the result of elemental analysis shows that there are five K^+ and two TMA^+ counter-cations, forming the formula $[(TMA)_2K_5(Nb_6P_2W_{12})_2Co_3(H_2O)_{11}O_{121}]^{5-}$. Therefore, the formula of **1** still requires five additional protons for charge balance. However, as stated by Nyman and us,[46] it is difficult to locate these five protons from the Fourier map because of the very large number of crystallographically independent atoms and variable parameters, as well as the presence of heavy atoms (Nb and W) and high mobility of the lattice species. In addition, we could not locate the position of five protons by BVS calculations owing to the distortion and asymmetry. We think the five charge-balancing protons are probably delocalized in the structure, and thus the actual formula of cluster **1a** is $(TMA)_2K_5[H_5(Nb_6P_2W_{12})_2Co_3(H_2O)_{11}O_{121}]\cdot 31H_2O$.

Infrared Spectroscopy. The Fourier transform infrared (FTIR) spectrum of **1** (Figure S6) shows characteristic absorptions of the Well−Dawson polyanion $Nb_6P_2W_{12}$. The broad band at 3406 cm^{-1} and strong peak at 1624 cm^{-1} correspond to O−H stretching modes, indicating the presence of the water molecules. The bands at 1083 and 1006 cm^{-1} are associated with P−O asymmetric stretching modes. The features at 954 and 903 cm^{-1} are attributed to terminal W═O and bridging W−O−W stretching modes, respectively. The broad band at 770 cm^{-1} originates from terminal Nb═O vibration, whereas the peaks at 692 cm^{-1} corresponds to bridging Nb−O−Nb(W) vibrations. In addition, the anionic charge of MAP $Nb_6P_2W_{12}$ unit is higher than that of the saturated P_2W_{18} parent species (Table S5), which results in a slight bathochromic shift of W−O vibrations in the FTIR spectrum of **1**. As shown in Figure 4, the IR spectrum of **1** is very similar to those of monomeric and dimeric MAP clusters, $K_{3.5}Na_4[H_{4.5}(NbO_2)_6P_2W_{12}O_{56}]\cdot 12.5H_2O$ ($P_2W_{12}(NbO_2)_6$, monomer) and $K_7[H_{13}\{Nb_6(O_2)_4P_2W_{12}O_{57}\}_2]\cdot 31H_2O$ (dimer). The main differences are (i) the phosphate stretch at ca. 1080 cm^{-1} for **1** and $P_2W_{12}(NbO_2)_6$ splits into two bands at 1058 and 1084 cm^{-1} for the dimer and (ii) the absence of weak peak around 870 cm^{-1}, indicating the complete transformation of peroxo groups into oxo groups in **1**. In addition, compound **1** is well characterized via UV−vis absorption spectroscopy (Figures S7 and S8), UV−vis diffuse reflectance spectroscopy (Figure S9), and thermogravimetric analysis (Figure S10), which are consistent with their supramolecular structures.

Mass Spectroscopy. The solution behavior of cluster **1a** was examined by ESI-MS analysis. The negative ion ESI mass spectrum of compound **1** shows three peaks centered at m/z 1126.17 (calcd 1126.14), 1335.82 (calcd 1335.54), and 1621.97 (calcd 1621.28), whose charges are −7, −6, and −5, respectively (Figure 5). It can be seen that the ESI-MS data of crystal **1** well matches with the formula of the compound and the simulated mass spectra (Table S6). The strongest peak with m/z value in the range of 1110−1150 can be ascribed to the overlap with a set of isotopic envelopes with charge of −7

https://dx.doi.org/10.1021/acs.inorgchem.9b03700
Inorg. Chem. 2020, 59, 6747−6754

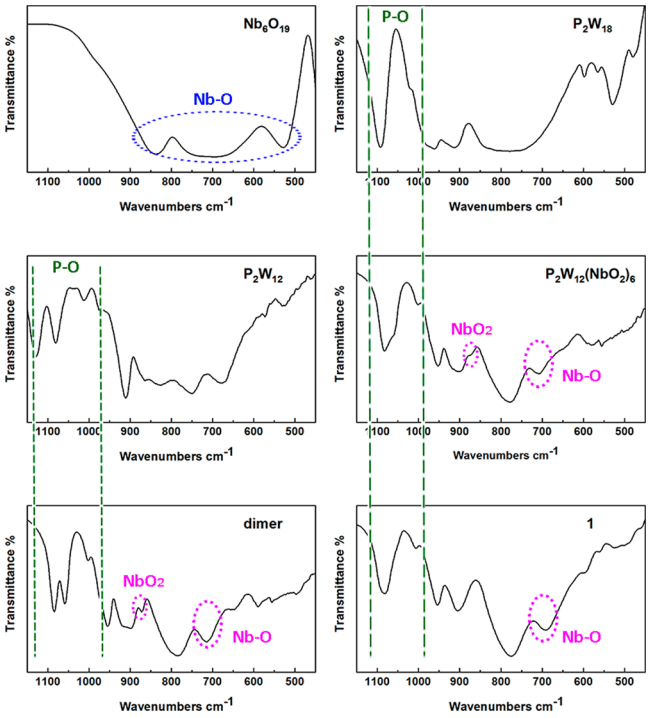

Figure 4. IR spectra for $K_7[HNb_6O_{19}]\cdot 13H_2O$ (Nb_6O_{19}), $K_6[\alpha\text{-}P_2W_{18}O_{62}]\cdot 14H_2O$ (P_2W_{18}), $K_{12}[H_2P_2W_{12}O_{48}]\cdot 24H_2O$ (P_2W_{12}), $K_{3.5}Na_4[H_{4.5}(NbO_2)_6P_2W_{12}O_{56}]\cdot 12.5H_2O$ ($P_2W_{12}(NbO_2)_6$), $K_7[H_{13}\{Nb_6(O_2)_4P_2W_{12}O_{57}\}_2]\cdot 31H_2O$ (dimer), and compound **1** in the region between 1150 to 450 cm^{-1}.

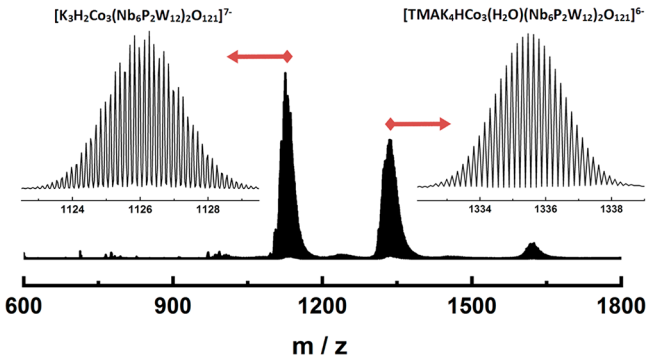

Figure 5. Molecular diagram and the negative-ion ESI mass spectrum of compound **1**, highlighting the expansion of the peak centered at 1126.17 and 1335.82 to show its 7- and 6- charge state, respectively.

(Figure S11). Assignments of these peaks suggest that they are all dimers of the same basic parent cluster $[Co_3(Nb_6P_2W_{12})_2O_{121}]^{12-}$ (dimeric cluster **1a**) with different numbers of TMA, H, and K counterions and water molecules, which suggests that the dimeric cluster retained its structural integrity in solution. Furthermore, time-resolved ESI-MS shows that the peaks of dimeric cluster **1a** remains nearly unchanged after 2 weeks, indicating its good stability in solution (Figure S12).

Solution Behavior. The incorporation of cobalt ions has shown its significance to manipulate the crystal structure into the 1D chain. In addition to the solid crystal, it is also intriguing to explore the effects of cobalt on solution behaviors. Unlike small ions (described by Debye−Hückel theory[47]) and large colloids particles (described by DLVO theory[48]), the POM clusters with nanometer-scale size and moderate charges show slow self-assembly behavior into hollow spherical, single-layered, blackberry-type structures in solution.[49] Generally, the size of assemblies will increase in solvents with lower polarity for the self-assembly controlled by counterion-mediated attraction,[50] while the functionalized ligands on POM surface can introduce other interactions to modulate the size tend versus solvent polarity.[51,52] In contrast to 1D chain-like structures in solid state, the chain will disassociate into isolated dimeric clusters **1a** in water. As measured from small-angle X-ray scattering (SXAS), the R_g value from 5.0 mg/mL sample solution is 7.53 Å (Figure S13), which indicates that the chain-like structures are not retained in solution. From the ESI-MS results (Figure 5), the chain will be dissociated into dimeric clusters, and each cluster contains three cobalt ions on the surface because of strong coordination between cobalt ions and active-sites of POM. From the time-resolved SLS measurements, the scattered intensity of solution shows a slow increase when the volume fraction of acetone varies from 65% to 85% (Figure 6a). After equilibrium of scattered intensity, the solution is still homogeneous. The CONTIN analysis[45] of DLS measurements (0.2 mg/mL in 75% water/acetone) shows that the size (R_h) of the assemblies is angular independent (Figure 6b) and close to the radius of hydration (R_g) measured from SLS (Figure S14), indicating the formation of hollow spherical assemblies. The average size (radius) of spheres obtained from TEM is 58 nm (Figure 6d), which agrees well with the R_h value from DLS.

When changing the solvent polarity to control the self-assembly process, the size of assemblies exhibits a more complicated trend, and with the increase of acetone volume fraction, the size will first increase then drop to smaller value (Figure 6c). The overall size trend here is quite similar to our previously reported one dominant by both counterion-mediated attraction and hydrogen bonding.[53] Beside the counterion-mediated attraction originating from the charged POMs, the cobalt ions with coordinated water ligands on the surface can provide additional hydrogen bonding to the self-assembly process. With the decrease of solvent polarity, the counterion-mediated attraction becomes stronger due to higher degree of POM-counterion association, while the hydrogen bonding is weaker in less polar solvents, which leads to the competition between two interactions and consequently results into this complicated size trend.

CONCLUSION

In conclusion, a novel, previously unknown $\{Nb_6P_2W_{12}\}$-based 1D chain cobalt derivative was synthesized, setting an example of the construction of MAP-based clusters. To accomplish the synthesis, the $\{(NbO_2)_6P_2W_{12}\}$ building block is first assembled in situ from simple inorganic precursors, followed by addition of cobalt salt and pH adjustment. The procedures do not require high temperatures necessary for hydrothermal conditions, and we think the general advantage of the developed approach is that it is reliable and simple, which could be used to design and synthesize novel MAP-based architectures with excellent properties. Also, the title compound represents the first MAP-based cobalt species known to date. Interestingly, the 1D chain architecture is disassociate into isolated dimeric clusters $[Co_3(Nb_6P_2W_{12})_2O_{121}]^{12-}$ in water. In addition, these charged clusters can self-assemble into blackberry-type structures in solution. Meanwhile, the cobalt also provides additional hydrogen bonding to control the self-assembly behavior. In

https://dx.doi.org/10.1021/acs.inorgchem.9b03700
Inorg. Chem. 2020, 59, 6747−6754

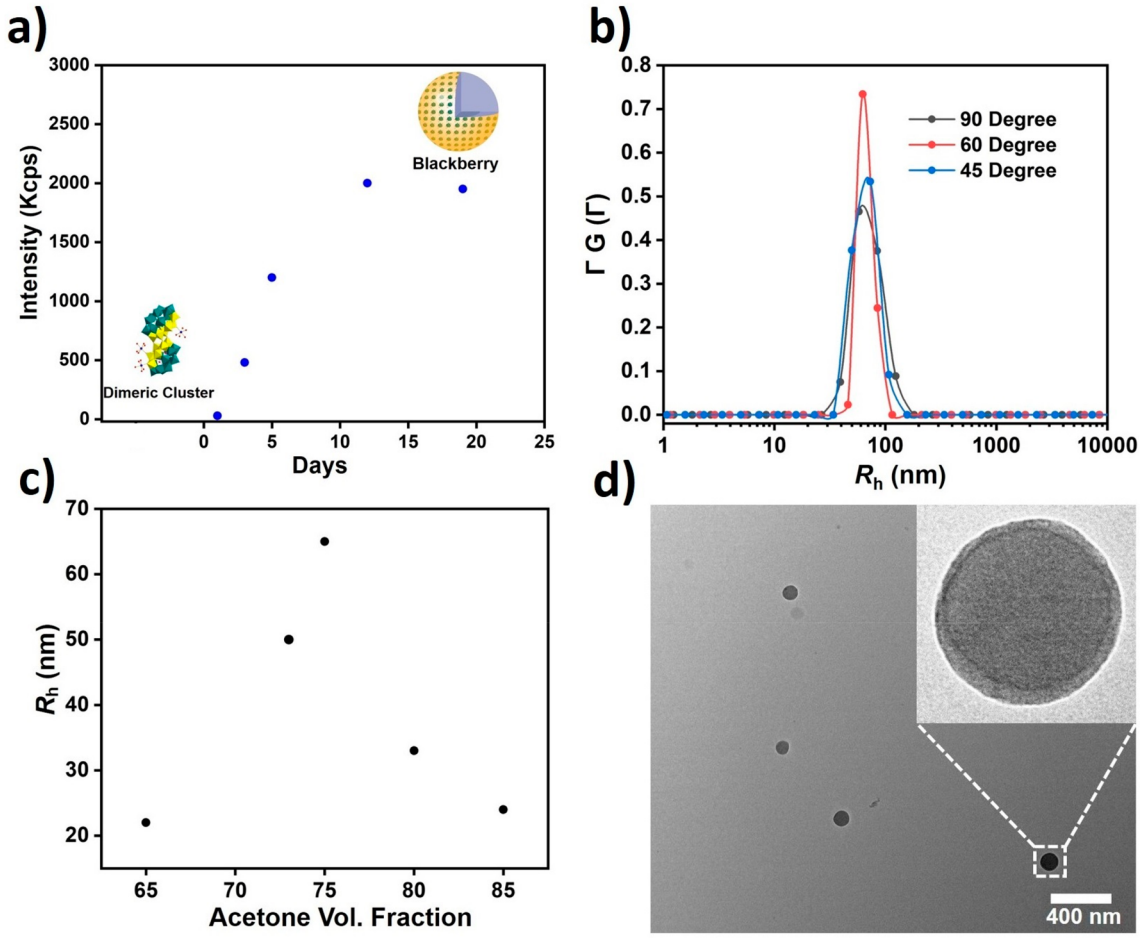

Figure 6. (a) The change of scattered intensity during the blackberry formation. (b) CONTIN analysis of 0.2 mg/mL cluster solution with 75% acetone volume fraction. The R_h is 66 nm. (c) The change of R_h at different volume fractions of acetone. (d) Representative TEM images from 75% acetone/water solutions. A zoom-in image shows the hollow nature of assemblies.

the future, we will explore the reactivity of $\{(NbO_2)_6P_2W_{12}\}$ toward the other 3d or 4f metals; it will also be interesting to see whether these Co-based assemblies of POMs have the photocatalysis capability to water-oxidation.

■ ASSOCIATED CONTENT

Supporting Information

The Supporting Information is available free of charge at https://pubs.acs.org/doi/10.1021/acs.inorgchem.9b03700.

Experimental section including material, synthesis, and instrumentation; BVS calculations of W, Nb, Co, and O atoms; additional structure diagrams; IR and UV spectra; TG curve; ESI-MS data; and related SLS curve, including Figures S1−S16 and Tables S1−S6 (PDF)

Accession Codes

CCDC 1915229 contains the supplementary crystallographic data for this paper. These data can be obtained free of charge via www.ccdc.cam.ac.uk/data_request/cif, or by emailing data_request@ccdc.cam.ac.uk, or by contacting The Cambridge Crystallographic Data Centre, 12 Union Road, Cambridge CB2 1EZ, UK; fax: +44 1223 336033.

■ AUTHOR INFORMATION

Corresponding Authors

Tianbo Liu − *Department of Polymer Science, The University of Akron, Akron, Ohio 44325, United States*; Email: tliu@uarkon.edu

Jingyang Niu − *Henan Key Laboratory of Polyoxometalate Chemistry, College of Chemistry and Chemical Engineering, Henan University, Kaifeng 475004, P. R. China*; orcid.org/0000-0001-6526-7767; Email: jyniu@henu.edu.cn

Authors

Dongdi Zhang − *Henan Key Laboratory of Polyoxometalate Chemistry, College of Chemistry and Chemical Engineering, Henan University, Kaifeng 475004, P. R. China*; orcid.org/0000-0002-2715-8591

Jiancheng Luo − *Department of Polymer Science, The University of Akron, Akron, Ohio 44325, United States*; orcid.org/0000-0002-3766-4922

Yachun Ma − *Henan Key Laboratory of Polyoxometalate Chemistry, College of Chemistry and Chemical Engineering, Henan University, Kaifeng 475004, P. R. China*

Tong Zhang − *Department of Polymer Science, The University of Akron, Akron, Ohio 44325, United States*

Nan Li − *Henan Key Laboratory of Polyoxometalate Chemistry, College of Chemistry and Chemical Engineering, Henan University, Kaifeng 475004, P. R. China*

https://dx.doi.org/10.1021/acs.inorgchem.9b03700
Inorg. Chem. 2020, 59, 6747−6754

Chen Li − *Henan Key Laboratory of Polyoxometalate Chemistry, College of Chemistry and Chemical Engineering, Henan University, Kaifeng 475004, P. R. China*
Pengtao Ma − *Henan Key Laboratory of Polyoxometalate Chemistry, College of Chemistry and Chemical Engineering, Henan University, Kaifeng 475004, P. R. China*
Tao Li − *Department of Chemistry and Biochemistry, Northern Illinois University, DeKalb, Illinois 60115, United States; X-ray Science Division, Advanced Photon Source, Argonne National Laboratory, Argonne, Illinois 60439, United States*
Guan Wang − *Henan Key Laboratory of Polyoxometalate Chemistry, College of Chemistry and Chemical Engineering, Henan University, Kaifeng 475004, P. R. China*
Jingping Wang − *Henan Key Laboratory of Polyoxometalate Chemistry, College of Chemistry and Chemical Engineering, Henan University, Kaifeng 475004, P. R. China*

Complete contact information is available at: https://pubs.acs.org/10.1021/acs.inorgchem.9b03700

Author Contributions

The manuscript was written through contributions of all authors. All authors have given approval to the final version of the manuscript.

Notes

The authors declare no competing financial interest.

■ ACKNOWLEDGMENTS

We are thankful for the financial support from the NSFC (21601056, 21371048) and the Program for Science & Technology Innovation Talents in Universities of Henan Province (19HASTIT044). T. Liu acknowledges support by the NSF (CHE1904397) and the University of Akron. T. Li appreciates startup support from Northern Illinois University. This research used resources of the Advanced Photon Source, a U.S. Department of Energy (DOE) Office of Science User Facility operated for the DOE Office of Science by Argonne National Laboratory under contract no. AC02-06CH11357.

■ REFERENCES

(1) Pope, M. T.; Müller, A. Polyoxometalate Chemistry: An Old Field with New Dimensions in Several Disciplines. *Angew. Chem., Int. Ed. Engl.* **1991**, *30*, 34−48.
(2) Müller, A.; Peters, F.; Pope, M. T.; Gatteschi, D. Polyoxometalates: Very Large Clusters Nanoscale Magnets. *Chem. Rev.* **1998**, *98*, 239−272.
(3) Long, D.-L.; Burkholder, E.; Cronin, L. Polyoxometalate Clusters, Nanostructures and Materials: From Self Assembly to Designer Materials and Devices. *Chem. Soc. Rev.* **2007**, *36*, 105−121.
(4) Cronin, L.; Müller, A. From Serendipity to Design of Polyoxometalates at the Nanoscale, Aesthetic Beauty and Applications. *Chem. Soc. Rev.* **2012**, *41*, 7333−7334 and the reference herein;.
(5) Du, D.-Y.; Yan, L.-K.; Su, Z.-M.; Li, S.-L.; Lan, Y.-Q.; Wang, E.-B. Chiral Polyoxometalate-based Materials: From Design Syntheses to Functional Applications. *Coord. Chem. Rev.* **2013**, *257*, 702−717.
(6) Rausch, B.; Symes, M. D.; Chisholm, G.; Cronin, L. Decoupled Catalytic Hydrogen Evolution from a Molecular Metal Oxide Redox Mediator in Water Splitting. *Science* **2014**, *345*, 1326−1330.
(7) Wang, S.-S.; Yang, G.-Y. Recent Advances in Polyoxometalate-Catalyzed Reactions. *Chem. Rev.* **2015**, *115*, 4893−4962.
(8) Bijelic, A.; Aureliano, M.; Rompel, A. Polyoxometalates as Potential Next-Generation Metallodrugs in the Combat Against Cancer. *Angew. Chem., Int. Ed.* **2019**, *58*, 2980−2999.
(9) Zhang, J.; Huang, Y.; Li, G.; Wei, Y. Recent Advances in Alkoxylation Chemistry of Polyoxometalates: From Synthetic Strategies, Structural Overviews to Functional Applications. *Coord. Chem. Rev.* **2019**, *378*, 395−414.
(10) Müller, A.; Beckmann, E.; Bögge, H.; Schmidtmann, M.; Dress, A. Inorganic Chemistry Goes Protein Size: A Mo368 Nano-Hedgehog Initiating Nanochemistry by Symmetry Breaking. *Angew. Chem., Int. Ed.* **2002**, *41*, 1162−1167.
(11) Long, D.-L.; Tsunashima, R.; Cronin, L. Polyoxometalates: Building Blocks for Functional Nanoscale Systems. *Angew. Chem., Int. Ed.* **2010**, *49*, 1736−1758.
(12) De la Oliva, A. R.; Sans, V.; Miras, H. N.; Yan, J.; Zang, H.; Richmond, C. J.; Long, D.-L.; Cronin, L. Assembly of a Gigantic Polyoxometalate Cluster $\{W_{200}Co_8O_{660}\}$ in a Networked Reactor System. *Angew. Chem., Int. Ed.* **2012**, *51*, 12759−12762.
(13) Dong, J.; Hu, J.; Chi, Y.; Lin, Z.; Zou, B.; Yang, S.; Hill, C. L.; Hu, C. A Polyoxoniobate-Polyoxovanadate Double-Anion Catalyst for Simultaneous Oxidative and Hydrolytic Decontamination of Chemical Warfare Agent Simulants. *Angew. Chem., Int. Ed.* **2017**, *56*, 4473−4477.
(14) Wu, Y.-L.; Li, X.-X.; Qi, Y.-J.; Yu, H.; Jin, L.; Zheng, S.-T. $\{Nb_{288}O_{768}(OH)_{48}(CO_3)_{12}\}$: A Macromolecular Polyoxometalate with Close to 300 Niobium Atoms. *Angew. Chem., Int. Ed.* **2018**, *57*, 8572−8576.
(15) Liu, J.-C.; Han, Q.; Chen, L.-J.; Zhao, J.-W.; Streb, C.; Song, Y.-F. Aggregation of Giant Cerium-Bismuth Tungstate Clusters into a 3D Porous Framework with High Proton Conductivity. *Angew. Chem., Int. Ed.* **2018**, *57*, 8416−8420.
(16) Xu, M.; Traustason, H.; Bo, F. D.; Hickam, S.; Chong, S.; Zhang, L.; Oliver, A. G.; Burns, P. C. Supramolecular Assembly of Geometrically Unstable Hybrid Organic−Inorganic Uranyl Peroxide Cage Clusters and Their Transformations. *J. Am. Chem. Soc.* **2019**, *141*, 12780−12788.
(17) Li, N.; Liu, J.; Liu, J.-J.; Dong, L.-Z.; Li, S.-L.; Dong, B.-X.; Kan, Y.-H.; Lan, Y.-Q. Self-Assembly of a Phosphate-Centered Polyoxo-Titanium Cluster: Discovery of the Heteroatom Keggin Family. *Angew. Chem., Int. Ed.* **2019**, *58*, 17260−17264.
(18) Dabbabi, M.; Boyer, M. Syntheses and Proprietes Hexaniobo-(V)-tungstates(VI). *J. Inorg. Nucl. Chem.* **1976**, *38*, 1011−1014.
(19) Finke, R. G.; Droege, M. W. Trisubstituted Heteropolytungstates as Soluble Metal Oxide Analogues. 1. The Preparation, Characterization, and Reactions of Organic Solvent Soluble Forms of $Si_2W_{18}Nb_6O_{77}^{8-}$, $SiW_9Nb_3O_{40}^{7-}$, and the $SiW_9Nb_3O_{40}^{7-}$ Supported Organometallic Complex $[(C_5Me_5)Rh)SiW_9Nb_3O_{40}]^{5-}$. *J. Am. Chem. Soc.* **1984**, *106*, 7274−7277.
(20) Edlund, D. J.; Saxton, R. J.; Lyon, D. K.; Finke, R. G. Trisubstituted Heteropolytungstates as Soluble Metal Oxide Analogues. 4.[la-c] The Synthesis and Characterization of Organic Solvent-Soluble $(Bu_4N)_{12}H_4P_4W_{30}Nb_6O_{123}$ and $(Bu_4N)_9P_2W_{15}Nb_3O_{62}$ and Solution Spectroscopic and Other Evidence for the Supported Organometallic Derivatives $(Bu_4N)_7[(C_5Me_5)Rh)P_2W_{15}Nb_3O_{62}]$ and $(Bu_4N)_7[(C_6H_6)Ru)P_2W_{15}Nb_3O_{62}]$. *Organometallics* **1988**, *7*, 1692−1704.
(21) Lu, Y.-J.; Lalancette, R.; Beer, R. H. Deoxygenation of Polynuclear Metal-Oxo Anions: Synthesis, Structure, and Reactivity of the Condensed Polyoxoanion $[(C_4H_9)_4N]_4(NbW_5O_{18})_2O$. *Inorg. Chem.* **1996**, *35*, 2524−2529.
(22) Kim, G.-S.; Zeng, H.; Rhule, J.; Weinstock, I.; Hill, C. Synthesis, X-Ray Structure, and Hydrolytic Chemistry of the Highly Potent Antiviral Polyniobotungstate A-α-$[Si_2Nb_6W_{18}O_{77}]^{8-}$. *Chem. Commun.* **1999**, No. 17, 1651−1652.
(23) Kim; Zeng; Van Derveer; Hill. A Supramolecular Tetra-Keggin Polyoxometalate. *Angew. Chem., Int. Ed.* **1999**, *38*, 3205−3207.
(24) Kim, G.-S.; Zeng, H.; Neiwert, W. A.; Cowan, J. J.; Van Derveer, D.; Hill, C. L.; Weinstock, I. A. Dimerization of A-α-$[SiNb_3W_9O_{40}]^{7-}$ by pH-Controlled Formation of Individual Nb-μ-O-Nb Linkages. *Inorg. Chem.* **2003**, *42*, 5537−5544.
(25) Li, S.-J.; Liu, S.-X.; Li, C.-C.; Ma, F.-J.; Liang, D.-D.; Zhang, W.; Tan, R.-K.; Zhang, Y.-Y.; Xu, L. Reactivity of Polyoxoniobates in Acidic Solution: Controllable Assembly and Disassembly Based on

Niobium-Substituted Germanotungstates. *Chem. - Eur. J.* **2010**, *16*, 13435−13442.
(26) Li, S.-J.; Liu, S.-X.; Ma, N.-N.; Qiu, Y.-Q.; Miao, J.; Li, C.-C.; Tang, Q.; Xu, L. Constructing Nanosized Polyanions with Diverse Structures by the Self-Assembly of W/Nb Mixed-Addendum Polyoxometalate and Lanthanide Ion. *CrystEngComm* **2012**, *14*, 1397−1404.
(27) Li, S.-J.; Liu, S.-X.; Li, C.-C.; Ma, F.-J.; Zhang, W.; Liang, D.-D.; Tan, R.-K.; Zhang, Y.-Y.; Tang, Q. Niobium-substituted Arsenotungstates: Controllable Transformation Between Monomers and Tetramer. *Inorg. Chim. Acta* **2011**, *376*, 296−301.
(28) Huang, P.; Qin, C.; Wang, X.-L.; Sun, C.-Y.; Jiao, Y.-Q.; Xing, Y.; Su, Z.-M.; Shao, K.-Z. Self-Assembly and Visible-Light Photocatalytic Properties of W/Nb Mixed-Addendum Polyoxometalate and Transition-Metal Cations. *ChemPlusChem* **2013**, *78*, 775−779.
(29) Wang, H.; Liang, Z.; Wang, Y.; Zhang, D.; Ma, P.; Wang, J.; Niu, J. Insight into the Reactivity of in Situ Formed $\{(NbO_2)_3SiW_9\}$: Synthesis, Structure, and Solution Properties of a Trimeric Polytungstosilicate Trapping a $\{MnNb_9\}$ Core. *Dalton Trans.* **2016**, *45*, 15236−15241.
(30) Wang, H.; Hou, L.; Li, C.; Zhang, D.; Ma, P.; Wang, J.; Niu, J. Synthesis, Structure, and Photocatalytic Hydrogen Evolution of a Trimeric Nb/W Addendum Cluster. *RSC Adv.* **2017**, *7*, 36416−36420.
(31) Judd, D. A.; Chen, Q.; Campana, C. F.; Hill, C. L. Synthesis, Solution and Solid State Structures, and Aqueous Chemistry of an Unstable Polyperoxo Polyoxometalate: $[P_2W_{12}(NbO_2)_6O_{56}]^{12-}$. *J. Am. Chem. Soc.* **1997**, *119*, 5461−5462.
(32) Ren, Y.; Hu, Y.; Shan, Y.; Kong, Z.; Gu, M.; Yue, B.; He, H. A Mixed-addenda Nb/W Polyoxometalate Containing Dimeric Dawson Subunit: Synthesis, Structure, and Characterization. *Inorg. Chem. Commun.* **2014**, *40*, 108−111.
(33) Zhang, D.; Liang, Z.; Xie, S.; Ma, P.; Zhang, C.; Wang, J.; Niu, J. A New Nb_{28} Cluster Based on Tungstophosphate, $[\{Nb_4O_6(OH)_4\}\{Nb_6P_2W_{12}O_{61}\}_4]^{36-}$. *Inorg. Chem.* **2014**, *53*, 9917−9922.
(34) Zhang, D.; Zhang, C.; Ma, P.; Bassil, B. S.; Al-Oweini, R.; Kortz, U.; Wang, J.; Niu, J. Two New Members of the Niobium-substituted Polytungstophosphate Family Based on Hexalacunary $[H_2P_2W_{12}O_{48}]^{12-}$ Building Blocks. *Inorg. Chem. Front.* **2015**, *2*, 254−262.
(35) Zhang, D.; Cao, F.; Ma, P.; Zhang, C.; Song, Y.; Liang, Z.; Hu, X.; Wang, J.; Niu, J. A $\{Nb_6P_2W_{12}\}$-Based Hexameric Manganese Cluster with Single-Molecule Magnet Properties. *Chem. - Eur. J.* **2015**, *21*, 17683−17690.
(36) Zhang, D.; Liang, Z.; Liu, S.; Li, L.; Ma, P.; Zhao, S.; Wang, H.; Wang, J.; Niu, J. Discovery of Heteropolytantalate: Synthesis and Structure of Two 6-Peroxotantalo-4-phosphate Clusters. *Inorg. Chem.* **2017**, *56*, 5537−5543.
(37) Li, D.; Ma, P.; Niu, J.; Wang, J. Recent Advances in Transition-metal-containing Keggin-type Polyoxometalate-based Coordination Polymers. *Coord. Chem. Rev.* **2019**, *392*, 49−80.
(38) Liang, Z.; Wu, H.; Singh, V.; Qiao, Y.; Li, M.; Ma, P.; Niu, J.; Wang, J. Assembly of Lanthanide-Containing Polyoxotantalate Clusters with Efficient Photoluminescence Properties. *Inorg. Chem.* **2019**, *58*, 13030−13036.
(39) Lv, H.; Song, J.; Geletii, Y. V.; Vickers, J. W.; Sumliner, J. M.; Musaev, D. G.; Koegerler, P.; Zhuk, P. F.; Bacsa, J.; Zhu, G.; et al. An Exceptionally Fast Homogeneous Carbon-Free Cobalt-Based Water Oxidation Catalyst. *J. Am. Chem. Soc.* **2014**, *136*, 9268−9271.
(40) Paille, G.; Gomez-Mingot, M.; Roch-Marchal, C.; Lassalle-Kaiser, B.; Mialane, P.; Fontecave, M.; Mellot-Draznieks, C.; Dolbecq, A. A Fully Noble Metal-Free Photosystem Based on Cobalt-Polyoxometalates Immobilized in a Porphyrinic Metal−Organic Framework for Water Oxidation. *J. Am. Chem. Soc.* **2018**, *140*, 3613−3618.
(41) Folkman, S. J.; Soriano-Lopez, J.; Galán-Mascarós, J. R.; Finke, R. G. Electrochemically Driven Water-Oxidation Catalysis Beginning with Six Exemplary Cobalt Polyoxometalates: Is It Molecular, Homogeneous Catalysis or Electrode-Bound, Heterogeneous CoOx, Catalysis? *J. Am. Chem. Soc.* **2018**, *140*, 12040−12055.
(42) Khenkin, A. M.; Somekh, M.; Carmieli, R.; Neumann, R. Electrochemical Hydroxylation of Arenes Catalyzed by a Keggin Polyoxometalate with a Cobalt(IV) Heteroatom. *Angew. Chem., Int. Ed.* **2018**, *57*, 5403−5407.
(43) Misra, A.; Kozma, K.; Streb, C.; Nyman, M. Beyond Charge Balance: Counter-Cations in Polyoxometalate Chemistry. *Angew. Chem., Int. Ed.* **2020**, *59*, 596−612.
(44) Hu, J.; Wang, Y.; Zhang, X.; Chi, Y.; Yang, S.; Li, J.; Hu, C. Controllable Assembly of Vanadium-Containing Polyoxoniobate-Based Three-Dimensional Organic−Inorganic Hybrid Compounds and Their Photocatalytic Properties. *Inorg. Chem.* **2016**, *55*, 7501−7507.
(45) Brown, I. D.; Altermatt, D. Bond-valence Parameters Obtained from a Systematic Analysis of the Inorganic Crystal Structure Database. *Acta Crystallogr., Sect. B: Struct. Sci.* **1985**, *41*, 244−247.
(46) Bontchev, R. P.; Nyman, M. Evolution of Polyoxoniobate Cluster Anions. *Angew. Chem., Int. Ed.* **2006**, *45*, 6670−6672.
(47) Debye, P.; Hückel, E. The theory of electrolytes. I. Lowering of freezing point and related phenomena. *Phys. Z.* **1923**, *24*, 185−206.
(48) Verwey, E. J. W.; Overbeek, J. T. G.; Van Nes, K. *Theory of the Stability of Lyophobic Colloids: The Interaction of Sol Particles Having an Electric Double Layer*; Elsevier Publishing Company: 1948.
(49) Liu, T. B.; Diemann, E.; Li, H. L.; Dress, A. W. M.; Muller, A. Self-assembly in Aqueous Solution of Wheel-shaped Mo-154 Oxide Clusters into Vesicles. *Nature* **2003**, *426*, 59−62.
(50) Kistler, M. L.; Bhatt, A.; Liu, G.; Casa, D.; Liu, T. A Complete Macroion-"Blackberry" Assembly-Macroion Transition with Continuously Adjustable Assembly Sizes in $\{Mo_{132}\}$ Water/Acetone Systems. *J. Am. Chem. Soc.* **2007**, *129*, 6453−6460.
(51) Haso, F.; Luo, J.; Bassil, B. S.; Artetxe, B.; Zhou, J.; Yin, P.; Reinoso, S.; Gutierrez-Zorrilla, J. M.; Kortz, U.; Liu, T. Effect of Directional Hydrogen Bonding on the Self-Assembly of Anisotropically-Shaped Macroions. *ChemistrySelect.* **2016**, *1*, 4345−4349.
(52) Haso, F.; Yang, P.; Gao, Y.; Yin, P.; Li, H.; Li, T.; Kortz, U.; Liu, T. Exploring the Effect of Surface Functionality on the Self-Assembly of Polyoxopalladate Macroions. *Chem. - Eur. J.* **2015**, *21*, 9048−9052.
(53) Provencher, S. W. CONTIN: A General Purpose Constrained Regularization Program for Inverting Noisy Linear Algebraic and Integral Equations. *Comput. Phys. Commun.* **1982**, *27*, 229−242.

https://dx.doi.org/10.1021/acs.inorgchem.9b03700
Inorg. Chem. 2020, 59, 6747−6754